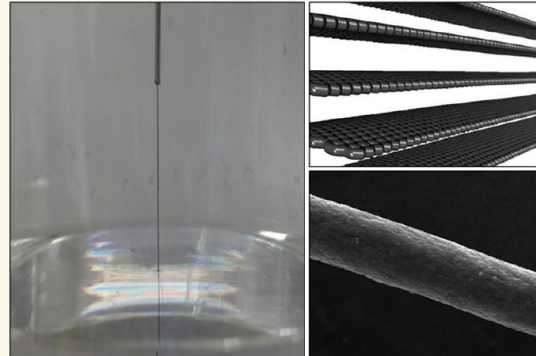


# Graphene Nanoribbons as an Advanced Precursor for Making Carbon Fiber

Changsheng Xiang,<sup>†,▲</sup> Natnael Behabtu,<sup>‡,▲,▼</sup> Yaodong Liu,<sup>†</sup> Han Gi Chae,<sup>†</sup> Colin C. Young,<sup>‡,§</sup> Bostjan Genorio,<sup>†</sup> Dmitri E. Tsentalovich,<sup>‡</sup> Chenguang Zhang,<sup>†,#</sup> Dmitry V. Kosynkin,<sup>†,▼</sup> Jay R. Lomeda,<sup>†</sup> Chih-Chau Hwang,<sup>†</sup> Satish Kumar,<sup>†,\*</sup> Matteo Pasquali,<sup>†,‡,||,\*</sup> and James M. Tour,<sup>†,‡,||,\*</sup>

<sup>†</sup>Department of Chemistry, <sup>‡</sup>Department of Chemical and Biomolecular Engineering, <sup>§</sup>Department of Physics, <sup>||</sup>Department of Mechanical Engineering and Materials Science, and the <sup>||</sup>Smalley Institute for Nanoscale Science and Technology, Rice University, 6100 Main Street, Houston, Texas 77005, United States, <sup>†</sup>School of Materials Science and Engineering, Georgia Institute of Technology, 801 Ferst Drive, NW MRDC-1, Atlanta, Georgia 30332-0295, United States, and <sup>#</sup>School of Materials Science and Engineering, Tianjin University, No. 92 Weijin Road, Tianjin, China 300072. <sup>▲</sup>These authors contributed equally to this work. <sup>▼</sup>Present address: DuPont Research, Wilmington, Delaware. <sup>||</sup>Present address: Saudi Arabian Oil Company, P.O. Box 21311, Dhahran, Saudi Arabia.

**ABSTRACT** Graphene oxide nanoribbons (GONRs) and chemically reduced graphene nanoribbons (crGNRs) were dispersed at high concentrations in chlorosulfonic acid to form anisotropic liquid crystal phases. The liquid crystal solutions were spun directly into hundreds of meters of continuous macroscopic fibers. The relationship of fiber morphology to coagulation bath conditions was studied. The effects of colloid concentration, annealing temperature, spinning air gap, and pretension during annealing on the fibers' performance were also investigated. Heat treatment of the as-spun GONR fibers at 1500 °C produced thermally reduced graphene nanoribbon (trGNR) fibers with a tensile strength of 378 MPa, Young's modulus of 36.2 GPa, and electrical conductivity of 285 S/cm, which is considerably higher than that in other reported graphene-derived fibers. This better trGNR fiber performance was due to the air gap spinning and annealing with pretension that produced higher molecular alignment within the fibers, as determined by X-ray diffraction and scanning electron microscopy. The specific modulus of trGNR fibers is higher than that of the commercial general purpose carbon fibers and commonly used metals such as Al, Cu, and steel. The properties of trGNR fibers can be further improved by optimizing the spinning conditions with higher draw ratio, annealing conditions with higher pretensions, and using longer flake GONRs. This technique is a new high-carbon-yield approach to make the next generation carbon fibers based on solution-based liquid crystal phase spinning.



**KEYWORDS:** graphene nanoribbon · fiber spinning · carbon fiber · coagulation

Polyacrylonitrile (PAN) and pitch are the two dominant precursors for the production of carbon fiber; each has its unique advantages, and fibers made from one raw material do not have the same properties as fibers made from the other. PAN-based carbon fiber is used for high tensile and compressive strength applications.<sup>1</sup> Because of processing ease, wet or dry jet wet spinning is used for PAN-based carbon fiber production.<sup>2,3</sup> PAN precursor fibers must be first postprocessed by oxidative stabilization at 200–300 °C in air, typically for 2–3 h, in order to convert PAN into an infusible ladder structure to enable the fibers to be stable during subsequent higher temperature processing.<sup>4–6</sup> The chemical reactions involved in the stabilization process are oxidation, cyclization, and dehydrogenation.<sup>7</sup>

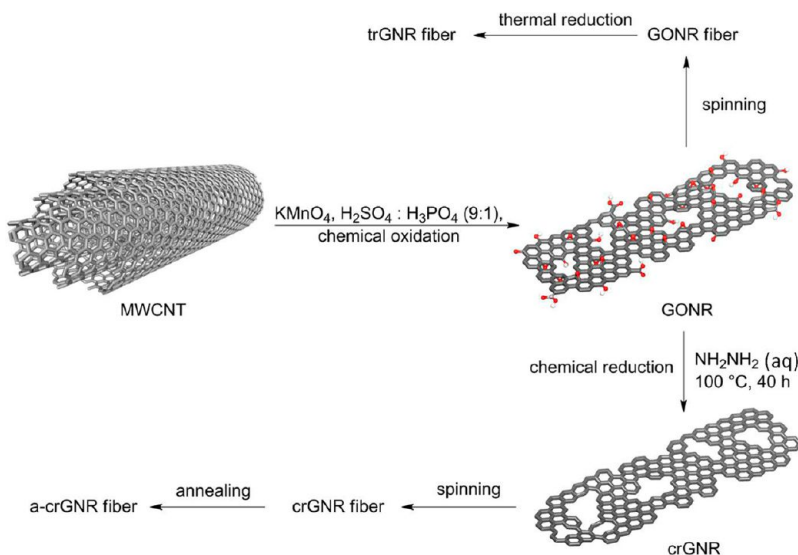
In the oxidation step, air acts as the oxidizing medium that produced a PAN backbone that bears oxygen functionality to give greater stability to the fiber at higher temperatures.<sup>8–10</sup> Cyclization of the nitrile groups with the adjacent carbons converts the C≡N to one C≡N and one C–N, thus forming a six-membered ring structure.<sup>11</sup> Dehydrogenation produces C=C by eliminating H atoms to stabilize carbon chains.<sup>12</sup> These stabilized fibers need to go through carbonization at  $\leq 1600$  °C in an inert atmosphere (nitrogen or argon) to eliminate the non-carbon atoms and form a turbostratic structure.<sup>7,13,14</sup> In order to achieve fiber orientation and high modulus, the carbonized fiber must undergo graphitization above 2100 °C to convert the turbostratic carbon structure to a graphite structure.<sup>7,15–17</sup> However, PAN contains highly polar nitrile

\* Address correspondence to satish.kumar@gatech.edu, mp@rice.edu, tour@rice.edu.

Received for review November 27, 2012 and accepted January 22, 2013.

Published online January 22, 2013  
10.1021/nn305506s

© 2013 American Chemical Society



**Scheme 1.** Procedure for processing two types of GNR fibers.

groups, which hinder the alignment of the molecular chains during spinning; thus the fibers are not completely graphitized during the graphitization process, yielding fibers with moderate modulus and electrical conductivity.<sup>17,18</sup>

Pitch-based carbon fibers can be classified into two categories according to their properties. High-performance carbon fiber (HPCF) is spun from anisotropic mesophase pitch, yielding fibers with high modulus and high electrical conductivity. General purpose carbon fiber (GPCF) is made from isotropic pitch, yielding moderate mechanical properties.<sup>19</sup> Mesophase pitch fibers yield high modulus and electrical conductivity because the intrinsic liquid crystal order of the spinning gel translates into well-aligned as-spun fibers that are ordered in three dimensions following heat treatment. Melt spinning is used for making mesophase pitch-based carbon fiber, and the spinning temperature is  $\sim 350\text{ }^{\circ}\text{C}$ .<sup>17,18,20,21</sup> Postprocessing of pitch-based carbon fiber is similar to that of PAN-based carbon fiber, as it also includes the same three steps including stabilization,<sup>22,23</sup> carbonization, and graphitization.<sup>18,24</sup>

The carbon yield of a carbon fiber precursor is the ratio of the weight of annealed product to the weight of the precursor, expressed as a percentage; precursors with a high carbon yield are crucial to carbon fiber production since usable content is optimized while producing less waste, thus lowering the production cost. Rayon, PAN, and pitch are three major precursors to carbon fiber production; they have carbon yields of 20–35, 50–60, and 70–80%, respectively.<sup>18,25</sup>

On the basis of the known properties of PAN and pitch-based carbon fibers, we conjectured that large mesogenic graphitic structures that are solution-spun at room temperature could be the ideal building blocks for making high-performance carbon fiber in a scalable, economical process. It is known that graphene forms

liquid crystals in superacid,<sup>26</sup> and that research has led to solution-spun mesogenic graphitic structure fibers.<sup>27</sup> Some work on GO liquid crystal formation has been done,<sup>28–32</sup> and the extrusion of the GO liquid crystal phase into a coagulation bath, followed by chemical reduction, produced graphene fiber.<sup>32,33</sup> Another method of making graphene fiber has been reported by baking GO aqueous suspension in a glass tube.<sup>34</sup> However, those graphene fibers were produced without intrinsic alignment, resulting in low tensile modulus and low electrical conductivity. More highly aligned fibers can be attained by applying drawing tension while spinning from liquid crystal solutions. Finally, the surface morphologies of the previously synthesized graphene fibers were not smooth, and they had a noncircular cross section. This likely could be solved by selecting an appropriate solvent for GO dispersion along with the proper matching coagulation bath solvent.

In this work, the starting materials for all fibers are graphene oxide nanoribbons (GONRs) that were obtained from the oxidative unzipping of multiwalled carbon nanotubes (MWCNTs).<sup>35,36</sup> The GONRs can be spun directly into GONR fibers. Those GONR fibers can be thermally reduced (tr) to yield trGNR fibers. By using hydrazine,<sup>35</sup> GONRs can be chemically reduced (cr) to crGNRs that can be spun into crGNR fibers. The crGNR fibers can be annealed (a) to afford a-crGNR fibers. The two different fiber preparations are shown in Scheme 1.

GONRs are an attractive precursor to carbon fiber, essentially combining the merits of PAN and pitch, as shown in Figure 1. GONRs are graphene layers with oxygen functional groups. The lengths of the GONRs average  $4\text{ }\mu\text{m}$ , with widths over 100 nm. In addition, both crGNRs and GONRs can be dispersed in chlorosulfonic acid, commonly used in manufacturing synthetic detergents, sulfonamide antibacterials, and pesticides,<sup>37</sup> to form anisotropic liquid crystal phases

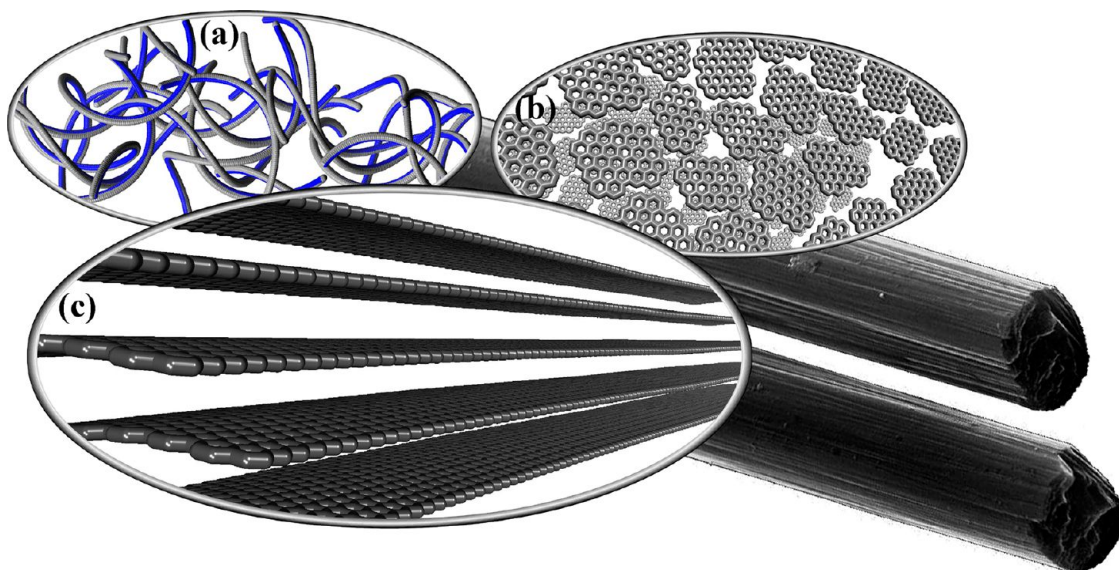


**Figure 1.** Schematic of the features of different carbon fiber precursors. (a) PAN precursor; long disordered polymer chains. (b) Mesophase pitch precursor; liquid crystal phase with small individual molecules about 2 nm in diameter. (c) GNR liquid crystal phase with individual ribbons 4  $\mu\text{m}$  in length, over 100 nm in width.

at room temperature. Diethyl ether ( $\text{bp} = 35^\circ\text{C}$ , viscosity = 0.224 cP at 25 °C) was used as the coagulation bath solvent. The spinning apparatus was the same as that used to spin carbon nanotube fibers;<sup>38,39</sup> it includes a self-made spinning chamber with a piston. The piston is connected to a pressure controller at one end of the chamber, and a spinneret (capillary tube) is affixed to the other end of the chamber. The lyotropic materials were extruded, through the small spinneret, into the coagulation bath with an air gap to produce aligned ribbons within the as-spun fibers. Stabilization is not necessary for crGNR or GONR fibers since they are already suitably constituted with preformed graphene layers. Carbon fibers produced from graphene nanoribbons (GNRs), after industrial optimization, might yield enhancements to this important class of materials, and we describe here our initial results using these starting structures.

## RESULTS AND DISCUSSION

**Solubility Study and Liquid Crystal Phase Observations.** The GONRs were characterized by SEM and atomic force microscopy (AFM) as shown in Figure S1 (Supporting Information). The average length of the ribbons was 4  $\mu\text{m}$ , and the width was >100 nm; a size distribution diagram is shown in Figure S1b. AFM analysis indicated that the height of the ribbon was ~1.2 nm, which implies that the ribbons are single layer.

The solubility of both GONRs and crGNRs in chlorosulfonic acid was studied prior to spinning. Microscope slides of 2 wt % GONRs or crGNRs were prepared for analysis by polarized optical microscope (POM). Birefringent patterns typical of a liquid crystal phase were detected from both samples (Figure 2). Concentrations of 8, 12, and 15 wt % GONR and 8 wt % crGNR samples were studied, and all had a liquid crystal phase

(Supporting Information Figure S2); this confirmed that GONRs and crGNRs are promising materials for solution-based wet spinning. However, 15 wt % GONRs start to show big aggregations which can deteriorate the spinning continuity and morphology of as-spun fibers. The GONRs and crGNRs are apparently dispersed in the acid through a protonation mechanism that is similar to that observed for graphene and SWNCTs.<sup>26,40,41</sup>

Raman spectroscopy of this GONR colloidal mixture showed a shift in the G peak from 1594.2 to 1618.1  $\text{cm}^{-1}$  (Supporting Information Figure S3), an indication of protonation by chlorosulfonic acid. This protonation is reversible since the Raman G peak shifted back to 1594.2  $\text{cm}^{-1}$  when the acid was washed away with water.

**Spinning Method and Parameters.** The spinning technique used is dry jet wet spinning, which is used by industry for PAN-based carbon fiber, Kevlar, and Zylon fiber spinning. Images of the spinning process, including extrusion with a 12 cm air gap, coagulation, and fiber collection are shown in Figure 3. The extrusion rate was 0.0066 mL/min; the length ( $L$ ) of the spinneret was 2.54 cm, and the orifice diameter ( $D$ ) was 125  $\mu\text{m}$ , so the  $L/D$  ratio was calculated to be 203. Tens of meters of continuous GONR fibers can be spun in 1 h. The air gap set here is crucial to the fiber's performance; this effect will be further discussed in the mechanical characterization section. The air gap has been observed to be very important for the spinability and drawability of some polymeric fibers, such as PAN; too long or too short an air gap will lead to inferior drawability and tensile properties. If a rolling drum is used to stretch the fiber during spinning, the alignment of the as-spun fiber can be further improved. Unfortunately, a higher draw ratio was not possible using the present apparatus; this problem could

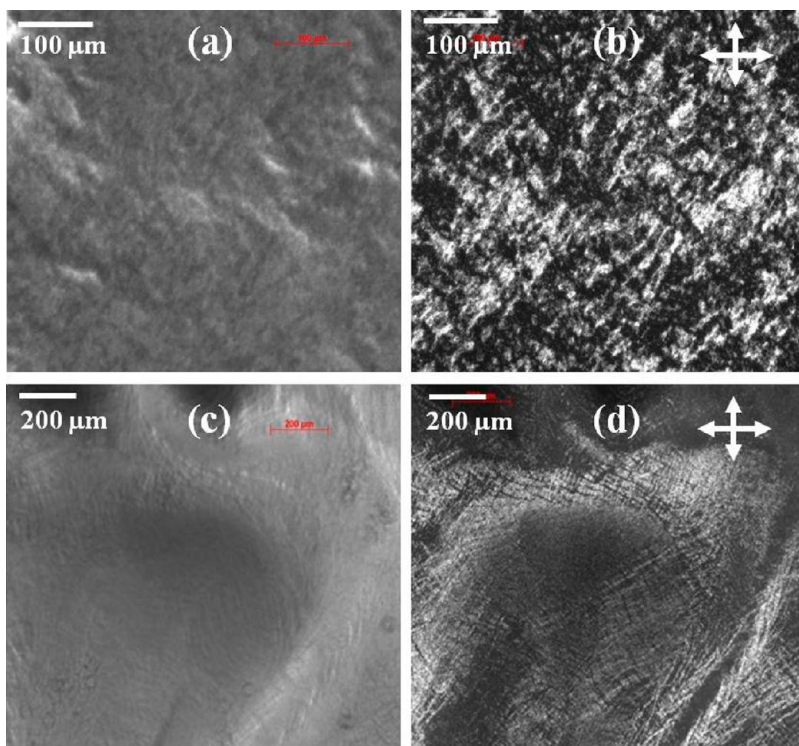


**Figure 2.** Liquid crystals in chlorosulfonic acid as observed through POM: (a) 2 wt % GONRs under transmission mode; (b) 2 wt % GONRs under cross-polarized mode; (c) 2 wt % crGNRs under transmission mode; (d) 2 wt % crGNRs under cross-polarized mode.

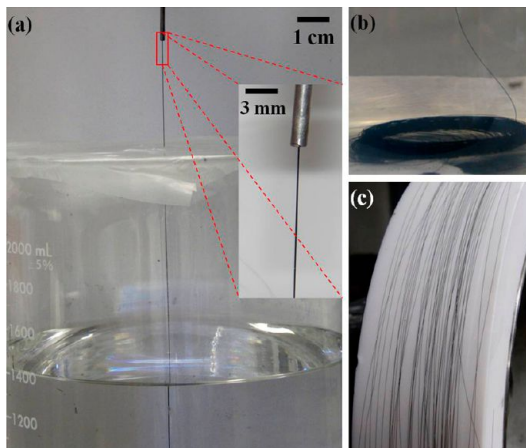


**Figure 3.** Dry jet wet spinning setup. (a) Coagulation bath of ether covered with parafilm to slow evaporation. Continuous fibers were spun into the bath with a 12 cm air gap. The area framed by the red box is enlarged in the inset image and shows the fiber extruding from the spinneret. (b) Fibers spontaneously form a coil in the bottom of the coagulation bath. (c) Fibers collected on a Teflon drum. A movie of the spinning process can be found in Supporting Information.

be solved by a newly engineered design. The maximum air gap for a stable spinning is 15 cm for the current setup.

**Coagulation and Fiber Morphology Study.** Little research has been done regarding the preferred coagulation bath conditions to produce graphene fibers, thus rough fiber morphologies and noncircular cross-sectional shapes were attained in previous studies.<sup>32,33</sup> The cross-sectional shape of wet-spun fibers is closely associated with the choice of coagulation conditions; it is an

important structural characteristic that can influence certain fiber and fiber assembly properties.<sup>42–44</sup> An appropriate coagulation bath composition should satisfy the needed requirements. First, GO or GONRs should be insoluble in the coagulation bath. Second, the cross-sectional shape of the wet-spun fibers is determined by the deformability of the coagulated layers and the mass transfer rate difference.<sup>43</sup> In other words, the coagulation rate should be high, thus the coagulated layers would have a small gradient at the interface between the surface layer and the core, and the coagulated outer layers will not deform easily toward the core direction, so a circular shape can be expected. The mass transfer rate difference needs to be low, which means the solvent's rate of diffusion out of the fiber should not be much faster than the absorption of the nonsolvent.<sup>44</sup> If the rates are not similar, then an irregular cross-sectional shape will likely be produced along with voids. Third, the viscosity of the bath should be low so as to mitigate etching of the surface of the fiber while it moves in the bath, therefore resulting in good surface morphology.

In this case, water was evaluated to make the GONR solution since water is easier and safer to use than chlorosulfonic acid. A liquid crystal phase was observed for a 5 wt % GONR aqueous solution, as shown in Figure S4a. For the coagulation bath, ethyl acetate, methyl acetate, or diethyl ether was tried, but none of these yielded satisfactory fiber morphologies, as shown in Figure S4b,c. Overall, dissolving the GONRs in water did not yield good fibers.

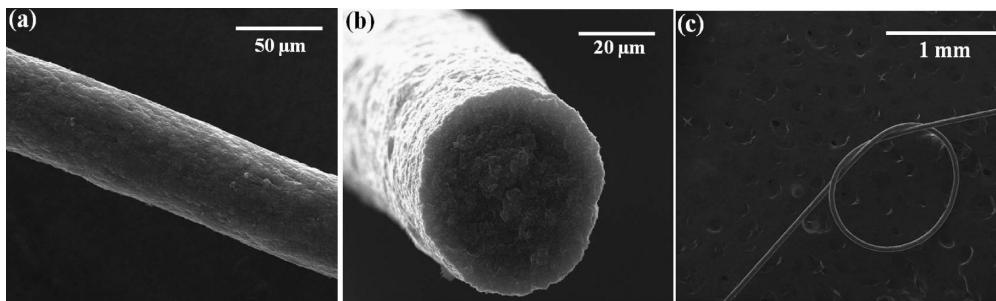


**Figure 4.** Characterizations of GONR fibers spun from 8 wt % colloid. (a) Surface morphology of the as-spun fiber. (b) Transverse cross-section morphology. (c) Fiber was knotted into a loop.

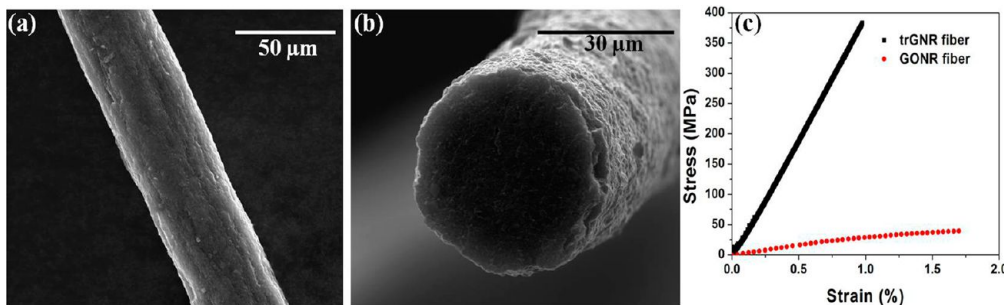


**Figure 5.** (a) Surface morphology of the 1050 °C annealed trGNR fiber. (b) Cross-section morphology of the 1050 °C annealed trGNR fiber. (c) Typical stress-strain curve of the as-spun GONR fiber (12 cm air gap) and 1050 °C annealed trGNR fiber (12 cm air gap) with 1.3 g of pretension.

SEM images of 8 wt % as-spun GONR fibers using the chlorosulfonic acid/diethyl ether solvent–coagulant pairs are provided in Figure 4, which shows circular cross-sectional shape.

**Mechanical Characterizations of GONR and trGNR Fibers from 8 wt % Colloid.** The GONR fibers spun with different air gaps have an average diameter of 54 μm, tensile strength of 33.2 MPa, modulus of 3.2 GPa, and elongation of 1.64%. GONR fibers are quite flexible and can be knotted into a loop with a minimum ~1 mm diameter, as shown in Figure 4c. The porosity of the as-spun GONR fiber was evaluated by using a BET measurement, and its  $N_2$  adsorption–desorption isotherm is shown in Figure S5. On the basis of the BET measurement, the fiber surface area is 58  $m^2/g$ .

Heat treatment of the precursor fibers is a key step for their improved performances. The moduli of both PAN and mesophase pitch-based carbon fiber increase with higher annealing temperature. The tensile strength of PAN-based carbon fiber peaks at a carbonization temperature of about 1500 °C and then drops upon further increase of carbonization temperature; for mesophase pitch-based carbon fiber, the tensile strength increases with higher annealing temperature.<sup>1</sup>

The surface morphologies of 1050 °C trGNR with 1.3 g force (gf) pretension are shown in Figure 5a,b. The diameter of the fiber was smaller since the oxygen functional groups and some voids were eliminated. The fiber with the best physical properties had a tensile strength of 383 MPa, a modulus of 39.9 GPa, and an elongation to break of 0.97%; a typical stress–strain

curve is shown in Figure 5c. The tensile strength and modulus increased by about 1 order of magnitude when compared to the as-spun GONR fibers. Higher molecular alignment leads to higher tensile modulus. Our result shows that trGNR fibers have higher tensile modulus when compared to graphene fibers produced using other methods (~10 GPa).<sup>32–34</sup> The density of trGNR fiber annealed without pretension was measured to be 0.88 g/cm<sup>3</sup>, less than half of that of carbon fibers (1.75–2.2 g/cm<sup>3</sup>).<sup>18</sup> This could be due to the existence of residual microvoids within the trGNR fibers. The specific strength of trGNR fiber is 430 kN\*m/kg, which is higher than some commercial GPCF and metals such as titanium, aluminum, and steel;<sup>45</sup> a comparison diagram is shown in Supporting Information Figure S6.

By comparing the performance of 1300 and 1500 °C trGNR fibers with 0.5 gf pretension, we observed that the tensile strength and modulus had a small increase; since this increase was within error limit, we can make no definite conclusion. The thermal annealing apparatus used in the present case has a high-temperature limit of 1500 °C; hence, no definite conclusions regarding temperatures above 1500 °C can be made.

The effect of the air gap on the properties of the fiber was also studied. As shown in Table 1, the GONR and trGNR fibers (8 wt %) with a 12 cm air gap had a significantly smaller diameter and better mechanical performance than the fibers with a 2 cm air gap. When a larger air gap was used, the gravity of extruded solution may accelerate the solution dripping speed

**TABLE 1. Processing Conditions and Mechanical Properties of GONR Fibers from Different Colloid Concentrations**

colloid concentration (wt %)	diameter <sup>a</sup> (μm)	pretension (gf)	annealing temperature (°C)	tensile strength (MPa)	Young's modulus (GPa)	elongation to break (%)
8 (2 cm air gap)	59.5 ± 1.6			25.1 ± 0.4	2.4 ± 0.2	1.40 ± 0.30
8 (12 cm air gap)	48.8 ± 3.4			39.3 ± 2.3	3.7 ± 0.3	1.82 ± 0.22
8	44.5 ± 2.1	0.3	1300	101.6 ± 7.1	8.4 ± 0.5	1.41 ± 0.13
8	40.4 ± 2.1	0.5	1300	151.7 ± 20.7	15.3 ± 1.0	1.02 ± 0.21
8	38.9 ± 0.4	0.5	1500	177.0 ± 17.0	15.4 ± 0.3	1.18 ± 0.11
8 (2 cm air gap)	32.2 ± 0.9	1.3	1050	200.5 ± 19.5	25.5 ± 0.1	0.85 ± 0.04
8 (12 cm air gap)	29.5 ± 0.6	1.3	1050	378.0 ± 5.0	36.2 ± 3.8	1.10 ± 0.13
12	72.1 ± 6.9			20.5 ± 2.1	3.2 ± 0.1	0.92 ± 0.03
15	82.0 ± 8.7			18.1 ± 7.2	1.7 ± 0.7	1.33 ± 0.01
15	56.2 ± 4.9	1	1300	210.6 ± 83.8	24.6 ± 4.0	0.82 ± 0.19

<sup>a</sup>Diameter was measured from the fracture surface through SEM observation.

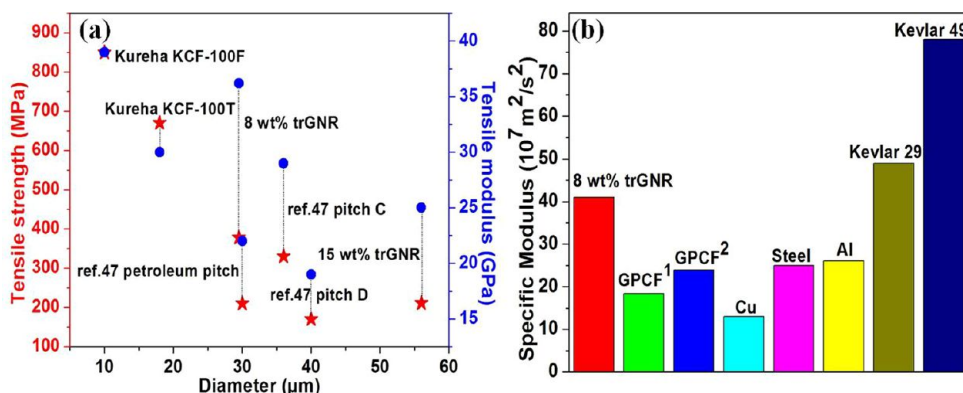


**Figure 6. Mechanical property comparisons of high-performance materials. (a)** Diagram of tensile strength and modulus versus fiber diameter of 8 and 15 wt % trGNR fibers and some GPCFs. **(b)** Comparison of the specific moduli of the trGNR fiber, GPCFs, metals, and Kevlar fibers. GPCF<sup>1</sup> refers to Kureha KCF-100T; GPCF<sup>2</sup> refers to Kureha KCF-100F.

before entering the coagulation bath, which stretches and further aligns the orientation of the GONR in the as-spun fibers. However, it is not true that lengthier air gap can always lead to better fibers. For a too long air gap, the axial elastic strain relaxation in the air gap would play a more important role than axial orientation in jet stretch. The optimal air gap in the current experimental setup was not investigated.

The application of pretension to the fiber during annealing should improve further the alignment of the trGNRs, resulting in improved electrical and mechanical properties. We therefore studied the effect of pretension on the performance of the fibers. Properties of trGNR fibers annealed up to 1500 °C with various pretensions are summarized in Table 1. Fibers produced using higher pretensions have better mechanical properties than the fibers annealed using low pretensions, an observation that has been made with the production of other carbon fibers.<sup>1</sup>

The tensile strength and modulus of trGNR fiber are slightly lower than those of the commercial GPCF<sup>46</sup> made by Kureha and comparable to the coal tar pitch-based GPCFs in the literature,<sup>47</sup> as shown in Figure 6a. It has been widely accepted that fibers with smaller diameters yield better mechanical properties due to the minimization of voids and defects within the fiber;

this can be supported by comparing the mechanical properties and SEM images of the transverse fracture morphology of trGNR fibers from 8 and 15 wt % colloids. Much better mechanical performance could be attained if the GNR fiber could be made smaller in diameter by using a smaller spinneret or a higher draw ratio while spinning. The smallest fiber diameter in the current study (Table 1) is about 29 μm, while the diameter of the current commercial high strength carbon fibers is in the range of 5–7 μm.

Specific modulus is a material property consisting of the elastic modulus divided by its density. High specific modulus is preferred in many applications such as airplane wings, masts, bicycle frames, and bridges whose design limitations are deflection and physical deformation. A diagram showing the specific modulus of different materials is shown in Figure 6b. The specific modulus of the trGNR fiber is  $41 \times 10^7 \text{ m}^2/\text{s}^2$ , higher than the commonly used metals such as steel, aluminum, and copper,<sup>45</sup> and is also higher than the commercial GPCFs produced by Kureha.<sup>46</sup> While its specific modulus is approaching that of Kevlar fiber,<sup>48</sup> it is still about 1 order of magnitude lower than the best HPCF.<sup>2</sup> Optimization of the spinning and annealing techniques would increase both the modulus and the tensile strength.

**X-ray Diffraction Study.** To study the structure and molecular alignment, X-ray diffraction (XRD) data for 8 wt % as-spun GONR and trGNR fibers are shown in Figure 7. The as-spun GONR fibers had two diffraction peaks at  $2\theta$  of  $\sim 10.2$  and  $42.7$ , which correspond to (002) and (100) planes, respectively. After heat treatment, compacted (002) graphene layers were formed and caused the diffraction peak to shift to  $2\theta \sim 25.9$ , which was clearly shown by the 2-D XRD detector images and the X-ray diffractograms.

Heat treatment under tension induces the packing and alignment of the ribbons along the fiber axis. Herman's orientation factor ( $f$ ) is defined by  $f = (3 \langle \cos^2 \phi \rangle - 1)/2$ ,

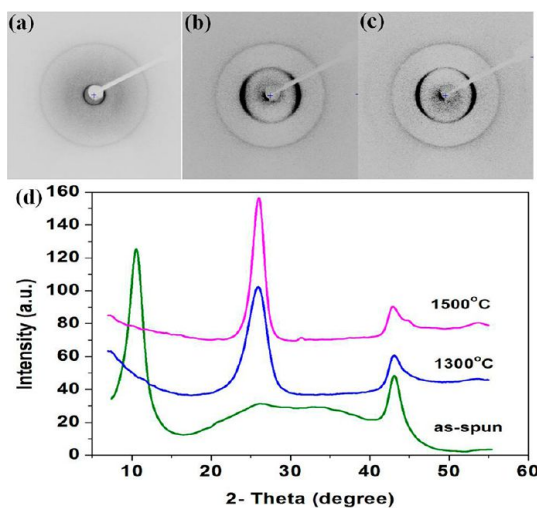


Figure 7. Two-dimensional XRD detector images of (a) as-spun 8 wt % GONR fiber; (b) 1300 °C annealed trGNR fiber; (c) 1500 °C annealed trGNR fiber. (d) X-ray diffractograms.

**TABLE 2. Parameters of Fibers Calculated Based on the XRD Data (They Are All from 8 wt % Colloidal Solution Spinning)**

sample name	$L_c$ (nm)	$d(002)$ (nm)	$f$	layer number
GONR	5.1	0.870	0.105	7
trGNR (1300 °C)	2.7	0.346	0.462	9
trGNR (1500 °C)	4.8	0.343	0.528	15

where  $\phi$  is the angle between the orienting entity and the fiber axis.<sup>49</sup> The optimized alignment of these ribbons was confirmed by observing Herman's orientation factor, which changed from 0.105 to 0.528 upon heat treatment. The crystal size ( $L_c$ ) was calculated by using Scherrer's formula;  $L_c$  increases along with higher annealing temperature. The value of the average graphene interlayer spacing  $d(002)$  was from Bragg's law;  $d(002)$  decreases with increased annealing temperature. The layer number is the number of graphene layers within a crystallite, which increases with higher annealing temperature.  $L_c$ ,  $d$  spacing, and layer numbers are summarized in Table 2; see Experimental Methods for calculations.

**Microstructure Study of Fibers before and after Heat Treatment.** Microstructures of the fibers before and after annealing were investigated, and the SEM images of fibers' transverse fracture surfaces are shown in Figure 8. For the as-spun fiber, the alignment of ribbons is poor, confirming that merely spinning fibers from a liquid crystal phase does not produce significant alignment if no draw tension or postprocessing is applied. In the 1300 °C trGNR fibers, large domains of partially ordered laminar structures were detected. During heat treatment, the arrangement of ribbons shifted from limited order to regional order; this phenomenon was confirmed by the previous XRD measurement where Herman's factor increased by 5 times. Heat treatment eliminated the oxygen functional groups on the GONRs. When pretensions were applied along the fiber axis direction, the ribbons also tended to rearrange toward that direction, thus inducing orientation within the fibers. Those regional ordered laminar structures can be further improved to well-ordered structures after spinning and heat treatment optimization studies.

**Electrical Properties.** The reduction of oxygen groups and alignment of ribbons both contribute to the large increase in the fiber's electrical conductivity. The 1500 °C treated trGNR fiber yielded a conductivity of 285 S/cm. This is higher electrical conductivity than that reported

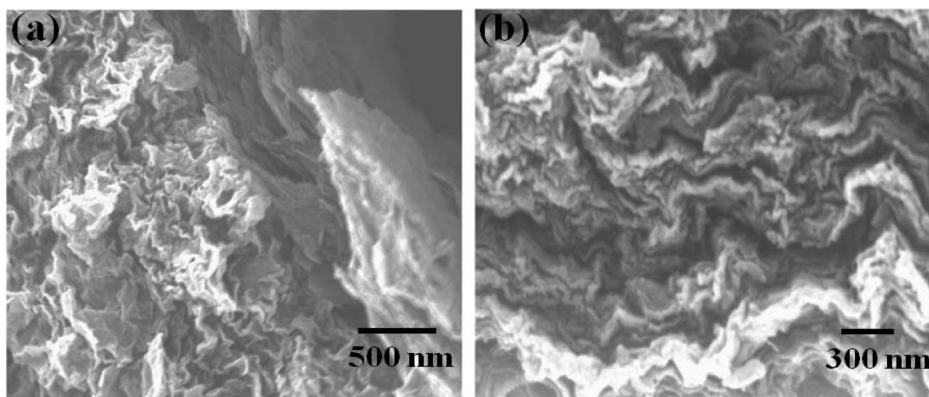
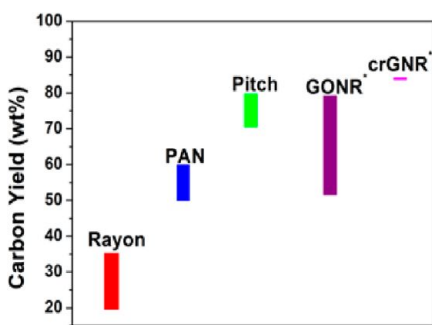


Figure 8. Transverse fracture surface of (a) as-spun GONR fibers from 15 wt % colloidal solution, showing ribbons with little order; (b) 1300 °C annealed trGNR fiber from 15 wt % colloidal solution with 1 gf of pretension, partially aligned graphitic layers.



**Figure 9.** Carbon yields of different carbon fiber precursors when heated over 2500 °C. \*Heated to only 950 °C in experiment; the additional weight loss between 1000 and 2500 °C is generally small.

for chemically reduced graphene fibers (250 S/cm<sup>32</sup> and 35 S/cm<sup>33</sup>) and the hydrothermally synthesized graphene fibers (10 S/cm).<sup>34</sup> Note that the GONRs used in current study are smaller in size than the GO flakes used in previous studies;<sup>32–34</sup> the smaller size usually leads to lower electrical conductivity. However, in our case, it is likely that the air gap during spinning and the pretension in the annealing process produce better fiber alignment that contributes to the better electrical properties. A typical *I*–*V* curve is shown in Figure S7.

**Fibers Spun from Other Concentrations.** GONR fibers spun from 12 and 15 wt % colloid solutions were characterized as was done for the 8 wt % fibers. Spinning from higher concentration yields fibers with larger diameters and lower tensile strength. Lower tensile strength results from more defects and voids within the fibers, and these defects and voids could easily initiate a break. The mechanical properties of fibers spun from the 12 and 15 wt % colloids are summarized in Table 1. Additional SEM images of the fiber morphology and their mechanical properties are shown in Figures S8–S10. The SEM images show that 15 wt % GONR fibers spun from the same batch exhibit large deviations in morphology and mechanical properties. This might be because the GONRs are near their upper solubility limit in chlorosulfonic acid. Spinning from 12 and 15 wt % colloids sometimes clogged the spinneret, and the fibers were not as continuous as those spun from the 8 wt % colloid.

**crGNR Fiber Spinning and Characterization.** Spinning of crGNR fibers was performed by the same process used for GONR fiber spinning. Since the crGNRs are quite conductive, even the as-spun crGNR fibers yield a

conductivity of 5.6 S/cm. Annealing a-crGNR fiber at 1050 °C without pretension yields a tensile strength of 90 MPa. The reason for the lower performance of the crGNR fiber compared to the trGNR is not clear. It is possible that there was poor dispersion of crGNR in chlorosulfonic acid at high concentration, leading to aggregation in the colloid and resulting in discontinuous spinning and more voids in the as-spun fibers. Images of the fiber morphology and its properties are shown in Figure S11.

**Carbon Yield.** Previous experiments indicated that the weight loss of 950 °C heated crGNRs was ~15 wt %.<sup>35</sup> Hence, the carbon yield of crGNRs is 85 wt % at this temperature. For GONRs, the carbon yield ranged from 52 to 80 wt % at 950 °C according to the oxidation level.<sup>35</sup> It is known that the weight loss in heat treating carbon materials over 1000 °C is mainly attributed to the loss of hydrogen,<sup>50,51</sup> which is less than 1 wt % even when heated to 3000 °C.<sup>52</sup> With that 1 wt % taken into account, the carbon yield of crGNR is still higher than any known carbon fiber precursors while the carbon yield of GONRs is comparable to that of PAN and pitch. A summary of the carbon yield of different precursors when heated over 2500 °C is shown in Figure 9.

## CONCLUSIONS

High concentrations of GONRs are dispersed in chlorosulfonic acid through a protonation mechanism. Continuous GONR fibers were successfully spun from liquid crystal phase solutions using an air gap in the spinning process. Fiber morphology and cross-sectional shape are directly related to the selection of coagulation bath solvent. Fibers spun from higher concentration yield more voids and lower performance. Postprocessing is crucial to achieve molecular alignment in a fiber. The GONR-based carbon fibers had better properties after higher temperature annealing with higher pretension. Partial anisotropic domains within the trGNR fiber matrix make their specific tensile strengths comparable to and their specific moduli and electrical conductivities higher than those of commercial GPCF. It is expected that far better properties can be attained by optimization of the spinning and annealing conditions to attain well-ordered fibers. This new carbon fiber precursor together with the more accessible spinning technique could be a harbinger for the next generation HPCF and spark a new advance for future carbon fiber production to serve the high-performance markets.

## EXPERIMENTAL METHODS

**Materials and Sample Preparations.** MWCNTs were of the endo-type and were generously donated by Mitsui & Co, Ltd. The MWCNTs were converted to GONRs using a previously published method.<sup>35</sup> For 8 wt % GONR colloidal solutions, GONRs (0.8 g) and chlorosulfonic acid (5.2 mL) were mixed in a flask in a glovebox and the flask was sealed using PTFE tape. The solution

was prepared in a hood following a protocol similar to that used for single-walled carbon nanotube solutions.<sup>38,39</sup> The colloid was returned to the glovebox again for microscope slide preparation. The slide must be sealed with aluminum tape to avoid its contact with air when it is removed from the glovebox for POM analysis. GONRs and crGNRs of other concentrations were made in a similar fashion using appropriate amounts of

materials. GONRs (0.8 g) were mixed with chlorosulfonic acid (3.3 or 2.6 mL) to get 12 or 15 wt % GONRs, respectively.

**Fiber Spinning and Processing.** GONR colloid was loaded into the spinning chamber within the glovebox. The loaded chamber was evacuated under vacuum before spinning to degas the sample. Fibers were extruded into the ether coagulation bath with an air gap of 2–15 cm (Supporting Information movie 1). Fibers were soaked in the bath for 10 min, collected on a rotating drum, and finally dried in the oven at 110 °C for 2 h.

**Heat Treatment.** For the heat treatment process, fiber specimens were fixed onto a graphite fixture under tension. The apparatus was purged with argon for 30 min at a flow rate of 14 L/min prior to heating. The samples were heated from room temperature to 1500 °C at a heating rate of 5 °C/min with purging argon at 10 L/min. After reaching the required temperature, it was held for 10 min and then the sample was cooled to room temperature.

**Mechanical Testing.** Mechanical testing was done using an Instron model 1000 with 0.5 mm/min extension rate and 12 mm gauge length. The diameter of the fiber was measured from the fracture surface by scanning electron microscopy (SEM) observation.

**Fiber Density Measurement.** Thirty meters of GONR fibers was collected and placed in the oven at 110 °C to remove the residual ether, followed by heat treatment at 1050 °C with no pretension. The cross-sectional area,  $S$ , of the fibers was obtained by SEM based on the average of 10 different samples. The weight of these fibers was determined using an Aldinger Mettler AE100 balance.

**X-ray Diffraction Measurement and Calculations.** Measurements were made by performing an equatorial scan (perpendicular to the fiber axis), a meridian scan (parallel to the fiber axis), and an azimuthal scan (rotating the fibers in the attachment) at the fixed Bragg position. The sample parameters were calculated as follows: the (002) peak from the equatorial scan was used to estimate the value of the average graphene interlayer spacing,  $d(002)$ , and the crystallite thickness  $L_c$ ; the layer number was obtained by using the formula  $L_c/d(002)$ . The value of  $d(002)$  was calculated using Bragg's law, and the crystallite thickness  $L_c$  was calculated using Scherrer's formula:  $d(002) = \lambda/2 \sin \theta; L_c = K\lambda/\beta \cos \theta$ , where  $\lambda$  is the X-ray wavelength,  $\theta$  is the scattering angle,  $K$  is the shape factor (0.89), and  $\beta$  is full width at half-maximum intensity.

**Conflict of Interest:** The authors declare no competing financial interest.

**Acknowledgment.** This work was supported by the Air Force Research Laboratory through University Technology Corporation, 09-S568-064-01-C1, the Air Force Office of Scientific Research (FA9550-09-1-0581, FA9550-09-1-0590, and FA9550-09-1-0150), the Air Force Office of Scientific Research MURI (FA9550-12-1-0035), the Office of Naval Research MURI Graphene Program (00006766, N00014-09-1-1066), and the Welch Foundation Grant C-1668.

**Supporting Information Available:** AFM images, POM images, Raman spectrum, additional mechanical test data, 2-D XRD detector image,  $I$ – $V$  curve, additional SEM images, and video of the spinning process. This material is available free of charge via the Internet at <http://pubs.acs.org>.

## REFERENCES AND NOTES

1. Morgan, P. *Carbon Fibers and Their Composites*; CRC Press: Boca Raton, FL, 2005.
2. Paul, D. R. A Study of Spinnability in the Wet-Spinning of Acrylic Fibers. *J. Appl. Polym. Sci.* **1968**, *12*, 2273–2298.
3. Grobe, V.; Mann, G. Structure Formation of Polyacrylonitrile Solutions into Aqueous Spinning Baths. *Faserforsch. Textiltech.* **1968**, *19*, 49–55.
4. Bajaj, P.; Roopanwal, R. K. Thermal Stabilization of Acrylic Precursors for Carbon Fibres: An Overview. *J. Macromol. Sci., Rev. Macromol. Chem.* **1997**, *37*, 97–147.
5. Damodaran, S.; Desai, P.; Abhiraman, A. S. Chemical and Physical Aspects of the Formation of Carbon Fibers from PAN-Based Precursors. *J. Text. Inst.* **1990**, *81*, 384–420.
6. Bashir, Z. A Critical Review of the Stabilisation of Polyacrylonitrile. *Carbon* **1991**, *29*, 1081–1090.
7. Rahaman, M. S. A.; Ismail, A. F.; Mustafa, A. A Review of Heat Treatment on Polyacrylonitrile Fiber. *Polym. Degrad. Stab.* **2007**, *92*, 1421–1432.
8. Ogawa, H.; Saito, K. Oxidation Behavior of Polyacrylonitrile Fibers Evaluated by New Stabilization Index. *Carbon* **1995**, *33*, 783–788.
9. Fitzer, E.; Frohs, W.; Heine, M. Optimization of Stabilization and Carbonization Treatment of PAN Fibres and Structural Characterization of the Resulting Carbon Fibres. *Carbon* **1986**, *24*, 387–395.
10. Dalton, S.; Heatley, F.; Budd, P. M. Thermal Stabilization of Polyacrylonitrile Fibres. *Polymer* **1999**, *40*, 5531–5543.
11. Beltz, L. A.; Gustafson, R. R. Cyclization Kinetics of Polyacrylonitrile. *Carbon* **1996**, *34*, 561–566.
12. Fitzer, E.; Muller, D. J. The Influence of Oxygen on the Chemical Reactions during Stabilization of PAN as Carbon Fiber Precursor. *Carbon* **1975**, *13*, 63–69.
13. Ko, T. H. The Influence of Pyrolysis on Physical Properties and Microstructure of Modified PAN Fibers during Carbonization. *Appl. Polym. Sci.* **1991**, *43*, 589–600.
14. Mittal, J.; Mathur, R. B.; Bahl, O. P. Post Spinning Modification of PAN Fibres—A Review. *Carbon* **1997**, *35*, 1713–1722.
15. Mittal, J.; Mathur, R. B.; Bahl, O. P. Single Step Carbonization and Graphitization of Highly Stabilized PAN Fibers. *Carbon* **1997**, *35*, 1196–1197.
16. Liu, J.; Wang, P. H.; Li, R. Y. Continuous Carbonization of Polyacrylonitrile-Based Oxidized Fibers: Aspects on Mechanical Properties and Morphological Structure. *Appl. Polym. Sci.* **1994**, *52*, 945–950.
17. Oberlin, A. Carbonization and Graphitization. *Carbon* **1984**, *22*, 521–541.
18. Minus, M. L.; Kumar, S. The Processing, Properties, and Structure of Carbon Fibers. *JOM* **2005**, *57*, 52–58.
19. Maeda, T.; Zeng, S. M.; Tokumitsu, K.; Mondori, J.; Mochida, I. Isotropic Pitch Precursor from Coal Tar by Air Blowing. *Carbon* **1993**, *31*, 407–412.
20. Singer, L. S. Union Carbide, High Modulus, High Strength Carbon Fibers Produced from Mesophase Pitch, U.S. Patent 4005183, 1977.
21. Singer, L. S. Carbon Fibers from Mesophase Pitch. *Fuel* **1981**, *60*, 839–847.
22. Lavin, J. G. Chemical Reactions in the Stabilization of Mesophase Pitch-Based Fibers. *Carbon* **1992**, *30*, 351–357.
23. Matsumoto, T.; Mochida, I. A Structural Study on Oxidative Stabilization of Mesophase Pitch Fibers Derived from Coal Tar Pitch. *Carbon* **1992**, *30*, 1041–1046.
24. Lafdi, K.; Bonnami, S.; Oberlin, A. Anisotropic Pitch-Based Carbon Fibers—Carbonization and Graphitization. *Carbon* **1992**, *30*, 533–549.
25. Matsumoto, T. Mesophase Pitch and Its Carbon Fibers. *Pure Appl. Chem.* **1985**, *57*, 1553–1562.
26. Behabtu, N.; Lomeda, J. R.; Green, M. J.; Higginbotham, A. L.; Sinitskii, A.; Kosynkin, D. V.; Tsvetkov, D.; Parra-Vasquez, A. N. G.; Schmidt, J.; Kesselman, E.; et al. Spontaneous High-Concentration Dispersions and Liquid Crystals of Graphene. *Nat. Nanotechnol.* **2010**, *5*, 406–411.
27. Tour, J. M.; Pasquali, M.; Behabtu, N.; Lomeda, J. R.; Kosynkin, D. V.; Duque, A.; Green, M. J.; Parra-Vasquez, N. A.; Young, C. Dissolution of Graphite, Graphite and Graphene Nanoribbons in Superacid Solutions and Manipulation Thereof. U.S. Patent 20120063988, 2010.
28. Xu, Z.; Gao, C. Aqueous Liquid Crystals of Graphene Oxide. *ACS Nano* **2011**, *5*, 2908–2915.
29. Kim, J. E.; Han, T. H.; Lee, S. H.; Kim, J. Y.; Ahn, C. W.; Yun, J. M.; Kim, S. O. Graphene Oxide Liquid Crystals. *Angew. Chem., Int. Ed.* **2011**, *50*, 3043–3047.
30. Dan, B.; Behabtu, N.; Martinez, A.; Evans, J. S.; Kosynkin, D. V.; Tour, J. M.; Pasquali, M.; Smalyukh, I. I. Liquid Crystals of Aqueous, Giant Graphene Oxide Flakes. *Soft Matter* **2011**, *7*, 11154–11159.
31. Aboutalebi, S. H.; Gudarzi, M. M.; Zheng, Q. B.; Kim, J. K. Spontaneous Formation of Liquid Crystals in Ultralarge

Graphene Oxide Dispersions. *Adv. Funct. Mater.* **2011**, *21*, 2978–2988.

32. Xu, Z.; Gao, C. Graphene Chiral Liquid Crystals and Macroscopic Assembled Fibres. *Nat. Commun.* **2011**, *2*, 571.
33. Cong, H.; Ren, X.; Wang, P.; Yu, S. Wet-Spinning Assembly of Continuous, Neat, and Macroscopic Graphene Fibers. *Sci. Rep.* **2012**, *2*, 613.
34. Dong, Z.; Jiang, C.; Cheng, H.; Zhao, Y.; Shi, G.; Jiang, L.; Qu, L. Facile Fabrication of Light, Flexible and Multifunctional Graphene Fibers. *Adv. Mater.* **2012**, *24*, 1856–1861.
35. Kosynkin, D. V.; Higginbotham, A. L.; Sinitskii, A.; Lomeda, J. R.; Dimiev, A.; Price, B. K.; Tour, J. T. Longitudinal Unzipping of Carbon Nanotubes To Form Graphene. *Nature* **2009**, *458*, 872–876.
36. Higginbotham, A. L.; Kosynkin, D. V.; Sinitskii, A.; Sun, Z.; Tour, J. M. Lower-Defect Graphene Oxide Nanoribbons from Multiwalled Carbon Nanotubes. *ACS Nano* **2010**, *4*, 2059–2069.
37. Cremlyn, R. J. *Chlorosulfonic Acid: A Versatile Reagent*; The Royal Society of Chemistry: Cambridge, U.K., 2002.
38. Ericson, L. M.; Fan, H.; Peng, H.; Davis, V. A.; Zhou, W.; Sulpizio, J.; Wang, Y.; Booker, R.; Vavro, J.; Guthy, C.; et al. Macroscopic, Neat, Single-Walled Carbon Nanotube Fibers. *Science* **2004**, *305*, 1447–1450.
39. Behabtu, B.; Young, C. C.; Tsentalovich, D. E.; Kleinerman, O.; Wang, X.; Ma, A. W. K.; Bengio, E. A.; ter Waarbeek, R. F.; de Jong, J. J.; Hoogerwerf, R. E.; et al. Strong, Light, Multifunctional Fibers of Carbon Nanotubes with Ultrahigh Conductivity. *Science* **2013**, *339*, 182–186.
40. Parra-Vasquez, A. N. G.; Behabtu, N.; Green, M. J.; Pint, C. L.; Young, C. C.; Schmidt, J.; Kesselman, E.; Goyal, A.; Ajayan, P. M.; Cohen, Y.; et al. Spontaneous Dissolution of Ultralong Single- and Multiwalled Carbon Nanotubes. *ACS Nano* **2010**, *4*, 3969–3978.
41. Davis, V. A.; Parra-Vasquez, A. N. G.; Green, M. M.; Rai, P. K.; Behabtu, N.; Prieto, V.; Booker, R. D.; Schmidt, J.; Kesselman, E.; Zhou, W.; et al. True Solutions of Single-Walled Carbon Nanotubes for Assembly into Macroscopic Materials. *Nat. Nanotechnol.* **2009**, *4*, 830–834.
42. Morton, W. E.; Hearle, J. W. S. *Physical Properties of Textile Fibers*; The Textile Institute: Manchester, U.K., 1978.
43. Ziabicki, A. *Fundamentals of Fiber Formation*; John Wiley & Sons: New York, 1976.
44. Liu, C. K.; Cuculo, J. A.; Smith, B. Diffusion Competition between Solvent and Nonsolvent during the Coagulation Process of Cellulose/Ammonia/Ammonium Thiocyanate Fiber Spinning System. *J. Polym. Sci., B: Polym. Phys.* **1990**, *28*, 449–465.
45. Meyers, M. A.; Chawla, K. K. *Mechanical Behavior of Materials*; Cambridge University Press: New York, 1999.
46. Kureha Carbon Products Brochure, <http://www.kureha.com/pdfs/Kureha-KRECA-Carbon-Fiber.pdf> (accessed September 25, 2012).
47. Alcañiz-Monge, J.; Cazorla-Amorós, D.; Linares-Solano, A.; Oya, A.; Sakamoto, A.; Hosm, K. Preparation of General Purpose Carbon Fibers from Coal Tar Pitches with Low Softening Point. *Carbon* **1997**, *35*, 1079–1087.
48. Kevlar Technical Guide II-1, Aramid Fiber, Dupont, [http://www2.dupont.com/Kevlar/en\\_US/assets/downloads/Technical%20Guide%20for%20KEVLAR\\_2011.pdf](http://www2.dupont.com/Kevlar/en_US/assets/downloads/Technical%20Guide%20for%20KEVLAR_2011.pdf) (accessed September 25, 2012).
49. Bhattacharyya, A. R.; Sreekumar, T. V.; Liu, T.; Kumar, S.; Ericson, L. M.; Hauge, R. H.; Smalley, R. E. Crystallization and Orientation Studies in Polypropylene/Single Wall Carbon Nanotube Composite. *Polymer* **2003**, *44*, 2373–2377.
50. Redmond, J. P.; Walker, P. L., Jr. Gas Content of Graphites. *Nature* **1960**, *186*, 72–74.
51. Meyer, R. T.; Lynch, A. W.; Freese, J. M.; Smith, M. C.; Impresia, R. J. Residual Hydrocarbon and Hydrogen Contents of Carbons and Graphites. *Carbon* **1973**, *11*, 258–260.
52. Mehrotra, B. N.; Bragg, R. H.; Rao, A. S. Effect of Heat Treatment Temperature on Density, Weight and Volume of Glass-like Carbon. *J. Mater. Sci.* **1983**, *18*, 2671–2678.